Available online at www.sciencedirect.com
ScienceDirect
Thin Solid Films 515 (2007) 3779–3786
thin solid films
www.elsevier.com/locate/tsf

Optimization of plasma-enhanced chemical vapor deposition silicon oxynitride layers for integrated optics applications

M.G. Hussein *, K. Wörhoff, G. Sengo, A. Driessen

Integrated Optical MicroSystems, MESA+ Research Institute, University of Twente, P.O. Box 217, 7500 AE Enschede, The Netherlands

Received 19 April 2006; received in revised form 8 September 2006; accepted 26 September 2006
Available online 7 November 2006

Abstract

Silicon oxynitride (SiO_xN_y:H) layers were grown from 2%SiH_4/N_2 and N_2O gas mixtures by plasma-enhanced chemical vapor deposition (PECVD). Layer properties such as refractive index, deposition rate, thickness non-uniformity and hydrogen bond content were correlated to the relevant deposition parameters including radio frequency power, chamber pressure, total gas flow, substrate temperature and N_2O/SiH_4 gas flow ratio. As a result, optimized SiO_xN_y:H layers could be produced over a wide index range (1.46–1.70) with good thickness uniformity and sufficiently high deposition rate. With a refraction index non-uniformity $<5\times10^{-4}$ a thickness non-uniformity could be obtained below 1% over a 70×70 mm^2 area of a 100 mm wafer at a deposition rate >50 nm/min. The material composition and the optical properties of the SiO_xN_y:H layers were characterized by spectroscopic ellipsometry, X-ray Photoelectron Spectroscopy, Fourier Transform Infrared spectroscopy and prism coupler techniques. A simple atomic valence model is found to describe the measured atomic concentrations for PECVD silicon oxynitride layers.

Keywords: Plasma-enhanced chemical vapor deposition; Silicon oxynitride; Process optimization; Layer composition; Optical properties

1. Introduction

In recent years, increasing attention has been paid to silicon based dielectrics such as silicon oxynitride (SiO_xN_y:H or shortly SiON) as a promising material for densely integrated optics [1–5]. This is mainly due to the possibility of obtaining high refractive index (n) contrast waveguiding structures for a broad wavelength range from visible to IR by changing the nitrogen/oxygen composition from SiO_2 ($n=1.46$) to Si_3N_4 ($n=2.0$). In practice preferentially use is made of plasma-enhanced chemical vapor deposition (PECVD) as it allows for relatively high deposition rates at low temperatures (<400 °C). The PECVD SiO_xN_y:H layers are mostly grown from nitrous oxide (N_2O) and silane (SiH_4/N_2) with optional an addition of ammonia (NH_3). In the present study a relation is established between the layer properties and the deposition process parameters. We will restrict ourselves to high frequency excitation of the plasma and, mainly because of its lower complexity [6], to the N_2O–SiH_4/N_2 system.

For integrated optics applications, the uniformity and reproducibility of the refractive index and the thickness of the layers are highly important parameters. The structural and optical properties, like the index and loss, of the PECVD SiO_xN_y:H layers are strongly dependent on the layer composition [7]. This, in turn can be controlled by the parameters of the PECVD process, like the flow rate and the ratio of the process gases, the chamber pressure, the radio frequency (RF) power and the substrate temperature. A serious drawback of the chosen deposition process is the incorporation of undesirable N–H and Si–H bonds in the layers [2,4–6], which significantly increase the optical loss in the spectral region of interest for telecom applications [2,4,5,8–10].

In this work, we focus on the correlation between the deposition parameters and the PECVD SiO_xN_y:H layer properties, in order to identify those trends which lead to materials properties optimized for integrated optics applications. Based on the optimized deposition parameters, a series of layers with a broad range of refractive index between 1.48 and

* Corresponding author. Tel.: +31 53 4892665; fax: +31 53 4893343.
E-mail address: m.g.hussein@ewi.utwente.nl (M.G. Hussein).

0040-6090/$ - see front matter © 2006 Elsevier B.V. All rights reserved.
doi:10.1016/j.tsf.2006.09.046

1.66 has been fabricated. The optical and compositional properties of this series of SiON samples have been characterized by spectroscopic ellipsometry, X-ray Photoelectron Spectroscopy (XPS), Fourier Transform Infrared (FTIR) spectroscopy and prism coupler techniques.

2. Experimental details

Silicon oxynitride layers have been deposited with an Oxford Plasmalab System 133 PECVD reactor. It consists of a process chamber in which two parallel plate electrodes of 210 mm diameter are placed horizontally with a spacing of 20 mm. The upper electrode is powered at a frequency of 13.56 MHz, via an automatic matching unit, which matches the impedance of the generator to that of the process chamber to ensure maximum power transfer. The upper electrode is also functioning as a showerhead for the gas inlet. The system is integrated with a load-lock wafer transporter, allowing fast system pump-down.

All layers were deposited on *p*-type <100> oriented 100 mm silicon wafers. In order to determine the optimum processing parameters for the SiON deposition process, the following set of input parameters has been established after a preliminary study:

- RF power: 20 W
- Chamber pressure: 120 Pa
- Total gas flow: 2500 sccm
- Substrate temperature: 300 °C
- Gas flow ratio: 54 for N_2O/SiH_4 (calculated from the flow rates of N_2O and the 2%SiH_4/N_2 mixture).

Thereafter a systematic variation of the parameters has been made within the parameter window given in Table 1. This study, which should result in a better understanding of the principal effects and the contribution of each parameter to the layer properties, was carried out according to Pearson's correlation method [11].

In order to allow high accuracy of all measurement, the layer properties have been optimized for each of the characterization techniques. The layer thickness (d) and the index of refraction n have been determined by spectroscopic ellipsometry (Woollam M44) on approximately 250 nm thin layers directly deposited on silicon wafers. The measurement error is approximately 2×10^{-3} in refractive index and 0.1% in layer thickness. The thickness non-uniformity (δd) and refractive index non-uniformity (Δn), which have been measured by single-wavelength ellipsometry (Plasmos 2000), are given by the half difference between maximum and minimum deviation of the thickness and refractive index values measured over a 70×70 mm^2 area with a 15×15 points grid on the 100 mm wafers. In order to obtain higher precision for n, also prism coupling measurements were performed with an accuracy better than 6×10^{-4}.

Table 1
Variation range of the PECVD deposition parameters used to optimize SiO_xN_y:H layers

Input parameter	Range of variation
RF power	20–100 W
Chamber pressure	93–147 Pa
Total gas flow	1666.7–3333.3 sccm
Substrate Temperature	300–400 °C
N_2O/SiH_4 gas flow ratio	19.4–75

The XPS measurements were carried out with a PHI Quantera Scanning ESCA (Electron Spectroscopy for Chemical Analysis) Microprobe. A monochromatic Al X-ray source ($h\nu=1486.6$ eV) at 26.4 W was used, with a beam diameter of 100 μm and a 45° take-off angle. High resolution spectra were acquired using pass energy of 112 eV and a step size of 0.1 eV. The total pressure in the main chamber during analysis was 1.6×10^{-10} Pa. The spectrometer was calibrated using the Au $4f_{7/2}$ peak position at 84.00 eV. The samples were analyzed after 6 min (~70 nm in depth) sputtering by Argon ions beam accelerated at 3 keV and beam current of 15 nA. None of the sample was affected by charging effect. The atomic concentration values of the layers were calculated from the ratio of the experimental core level areas with PHI Multipak software version 8 (Physical Electronics, 2003) using factory calibrated values for the sensitivity factors of the respective elements (0.368, 0.733 and 0.499 for Si 2p, O 1s and N 1s respectively). For a detailed analysis of the chemical state of the elements within the layers, the core-level spectra were deconvolved revealing the contribution of different chemical environments. The XPS peaks were fitted by Gaussian–Lorentzian functions.

The bonding configuration and the hydrogen concentration were determined with a Digilab FTS-575C FTIR spectrometer with 1200 nm thick layers directly deposited onto the silicon substrates. The measurements were carried out at room temperature in a nitrogen atmosphere by infrared transmission through the deposited layer and the silicon substrate with a resolution of 4 cm^{-1}. The background has been subtracted by using an uncoated silicon substrate as reference. The hydrogen concentration of the layers was evaluated from the IR peak area of the N–H and Si–H peak applying the calibration factors from Lanford and Rand [12].

For optical loss measurements, all layers have been deposited on thermally oxidized silicon wafers. The thickness of the thermal oxide has been chosen sufficiently thick (~3.2 μm) so that the silicon substrate does not influence the modes. The measurements were performed on the fundamental mode using the sliding prism method [13] with an accuracy of approximately 0.2 dB/cm.

3. Results and discussion

3.1. Deposition mechanism

In the deposition chamber, electrons in the plasma gain energy by the RF electric field. These energetic electrons then transfer their energy to gas molecules by electron-impact collisions, resulting in molecular excitation, dissociation, and ionization. In this way, highly reactive chemical species are produced that enable deposition of films at low temperatures.

The deposition mechanisms for a PECVD process can be considered to consist of five major steps [14,15]:

Step 1 includes the primary initial electron-impact reactions between electrons and reactant gases to form ions and radical

Table 2
Strength of chemical bonds occurring during plasma deposition of SiO_xN_y:H

Chemical bonds	Bond strengths (kJ/mol)
Si–O	799.6
Si–N	470.0
Si–Si	325.0
Si–H	299.2
N–H	339.0
O–H	427.6

reactive species. The electron-impact ionization and dissociation of silane and nitrous oxide molecules can be written by the following equations [14,16]:

$$\begin{aligned} &e + SiH_4 \rightarrow SiH_m^+ + (4-m)H + e + e \quad m = 1,2,3 \\ &e + N_2O \rightarrow N_2 + O^+ + e + e \\ &e + N_2O \rightarrow NO^+ + N + e + e \end{aligned} \tag{1}$$

$$\begin{aligned} &e + SiH_4 \rightarrow SiH_m + (4-m)H + e \quad m = 1,2,3 \\ &e + N_2O \rightarrow N_2 + O + e \\ &e + N_2O \rightarrow NO + N + e \end{aligned} \tag{2}$$

Step 2 is dealing with the gas phase reaction and transport of the reactive species by diffusion to the wafer surface. The complex electro-chemical reactions which take place during the plasma deposition do not allow a detailed description. Instead we will focus on the gas molecules dissociation when utilizing N_2O and SiH_4/N_2 gaseous mixtures and describe the most favorable chemical reactions. The plasma contains SiH_m, O and N radicals, which can react to form energetically favorable bonds.

According to Table 2 [17], the most favorable chemical reaction is between SiH_m and O radicals leading to the formation of Si–O bonds. Thus, for large N_2O:SiH_4/N_2 flow ratios with an excess of O radicals in comparison with SiH_m radicals, only Si–O bonds will be formed. For decreasing flow ratios, the number of SiH_m radicals per O radical will increase, leading to oxygen deficiency, and thus to appearance of Si–N and Si–H bonds in the layers. However, decreasing the flow ratio even further leads to a deficiency of both oxygen and nitrogen radicals. Thus, homonuclear SiH_m reactions become favorite leading to silicon rich SiO_xN_y:H [18].

Step 3 is the adsorption of reactive species on wafer surface sites. There they can react with surface atoms or with other adsorbed species. The chemical reactions at the surface can be enhanced by ion bombardment. The coexistence of Si–H, N–H and Si–OH bonds offer the possibility for eliminating H_2 and H_2O [19,20]. In this way additional Si–N, Si–Si and Si–O–Si can be formed on the surface through the following reactions [20,21]:

$$\begin{aligned} &Si{-}H + N{-}H \rightarrow Si{-}N + H_2^{\nearrow} \\ &Si{-}H + Si{-}H \rightarrow Si{-}Si + H_2^{\nearrow} \\ &Si{-}H + Si{-}OH \rightarrow Si{-}O{-}Si + H_2^{\nearrow} \\ &Si{-}OH + Si{-}OH \rightarrow Si{-}O{-}Si + (H_2O)^{\nearrow} \end{aligned} \tag{3}$$

Step 4 takes into account the surface diffusion of the adsorbed species and reaction products. By diffusion nuclei will form islands and islands will merge to form a continuous thin film.

Step 5, finally, deals with desorption of the volatile reaction products, such as H_2 and H_2O vapor. Gaseous byproducts diffuse and flow out of the reactor.

3.2. Process optimization by correlation analysis

The objective of our investigation is to optimize the PECVD SiON deposition process over a wide index range (1.46–1.7) to arrive at layers with thickness uniformity within 1% and a deposition rate sufficiently high for technical applications (>50 nm/min). All layers have shown excellent refractive index in-homogeneity (Δn) below 2×10^{-3}, the accuracy of the scanning ellipsometer. Measurement by prism coupling of similar layers revealed a typical value of 5×10^{-4} (see also Ref. [4]). Pearson's correlation method is used to arrive at a detailed understanding of the deposition process leading eventually to optimized layers. In this section an overview is given of the experiments needed for the correlation analysis.

This analysis is carried out by changing systematically the process parameters of Table 1 and observing the influence on the refractive index (n), deposition rate (R) and thickness non-uniformity (δd) of the layers. Table 3 shows the resulting correlations with range between −1.00 to +1.00. A value −1.00 represents a perfect negative correlation for two variables, while +1.00 represents a perfect positive correlation. A value of 0.00 represents a total lack of correlation [11].

From the correlation results (Table 3) the following conclusions can be drawn:

- The RF power, the pressure and the total gas flow have a significant effect on the layer properties (n, R and δd). The N_2O/SiH_4 gas flow ratio has only a weak influence on δd and significant effect on n and R. The substrate temperature has only a minor effect to the layer properties within the range studied.
- The RF power shows a positive correlation with the deposition rate, thickness non-uniformity and a negative one with the refractive index; that means that R and δd increase and n decreases with increasing power. The increase of the deposition rate at higher RF power, while the partial pressure for both, silane and nitrous oxide, is kept constant, can be attributed to the increase of the concentration of the active reaction species and the plasma density with the power. The observed decrease of the refractive index at higher power can be understood when the dissociation efficiencies of both gases are taken into account. It is well known that silane has

Table 3
Correlation analysis results relating the PECVD input deposition parameters with the deposited SiO_xN_y:H layers properties (n, R and δd)

Input	Output		
	n	R	δd
RF power	−0.943	0.963	0.979
Pressure	−0.984	0.958	−0.997
Total flow ($2\%SiH_4/N_2+N_2O$)	0.977	0.982	−0.584
Substrate temperature	−0.347	0.102	0.456
Flow ratio (N_2O/SiH_4)	−0.918	0.784	−0.263

Table 4
N_2O/SiH_4 gas flow, refractive index (real n, and imaginary part k), deposition rate and thickness non-uniformity of the 5 different SiO_xN_y:H layers studied

Sample	N_2O/SiH_4 gas flow ratio	λ=632.8 nm		$R\pm\Delta R$ (nm/min)	δd (%)
		$n\pm\Delta n$	k		
S1	75.0	1.4871±0.0016	0	62.64±0.19	1.00
S2	39.3	1.5129±0.0018	0	67.41±0.20	0.86
S3	28.1	1.5322±0.0019	0.0020	65.55±0.20	0.92
S4	19.4	1.5690±0.0019	0.0032	61.93±0.18	0.93
S5	12.5	1.6525±0.0022	0.0045	55.36±0.17	1.08

higher dissociation efficiency than nitrous oxide [22] resulting in an domination of silane radicals at low power. By increasing the power, the relative concentration of oxygen radicals increases (see step 1) leading to a decrease of the refractive index.

- The chamber pressure shows a negative correlation with the refractive index and the thickness non-uniformity and a positive correlation with the deposition rate. At higher total pressure, the discharge voltage increases, making it difficult to start the plasma, since the impedance between the parallel plates decreases due to the higher gas concentration [23]. This results in a material with low density or a low refractive index with increasing pressure. On the other hand, the residence time increases by increasing the total pressure. This explains the increase in the deposition rate with increasing total pressure.
- Both refractive index and deposition rate increase with increasing total gas flow. It is clear that the residence time decreases by increasing the total gas flow. Since the silane has higher dissociation efficiency than nitrous oxide, this leads to domination of silane radicals that increase the refractive index. The discharge is sustained by electrons making ionizing collisions in the gas [23]. The number of ionizing collisions will increase with increasing gas density (total gas flow) leading to increase of the deposition rate.
- The substrate temperature, studied in the range 300 to 400 °C with a gas flow ratio (N_2O/SiH_4=54) shows only a weak influence on the layer properties. This could be expected as the mean electron energy or electron temperature is much higher than the substrate temperature [20]. Our results confirm that in the experimental regime under investigation the electron-impact ionization and dissociation (Eqs. (1) and (2)) is independent of the substrate temperature.
- The gas flow ratio (N_2O/SiH_4) correlates negatively with the refractive index and thickness non-uniformity and positively with the deposition rate. When the N_2O/SiH_4 flow ratio increases, the excited oxygen atom density increases too, leading to increasing disiloxane compared to the SiH_2 and SiH_3 precursors. As a result the formation of Si–O becomes favored leading to a layer composition close to SiO_2 (step 2). When the N_2O/SiH_4 flow ratio decreases, the incorporation of nitrogen and silicon in the form of Si–H, Si–N, N–H and Si–Si becomes more probable, leading, as expected, to an increasing refractive index. The increase of the deposition rate with increasing N_2O/SiH_4 flow ratio is expected, as we suppose that our deposition conditions give rise to a complete dissociation of the silane and that the process is limited by the nitrous oxide concentration.

Based on the correlation analysis, the optimal deposition conditions were selected to be: RF power 20 W, chamber pressure 140 Pa, total gas flow 2500 sccm and deposition temperature 350 °C. Since the N_2O/SiH_4 gas flow ratio does not influence the thickness non-uniformity significantly but has a large impact on the refractive index, this input parameter will be varied in order to study the properties of silicon oxynitride films with different composition in more detail.

3.3. Properties of optimized SiON layers

In this section we will show detailed results on the compositional and optical properties of various SiO_xN_y:H layer deposited under optimized processing conditions. The basic properties (optical constants, deposition rate and thickness uniformity) of five sets of layers (S1 to S5) that have been prepared by varying the N_2O/ SiH_4 input ratio are shown in Table 4. As can be seen, high quality SiO_xN_y:H layers could be obtained for a wide range of index of refraction with sufficiently high deposition rate and excellent uniformity.

The atomic ratios of Si, O and N in the layers were determined by XPS from the corrected areas of the Si 2p, N 1s, and O 1s peaks. Table 5 summarizes the binding energies of the photoelectron peaks and the atomic concentrations ratio of the deposited SiO_xN_y:H layers. The relative concentrations were determined to an accuracy of ~10% for silicon, oxygen and nitrogen with a detection limit of ~0.1 atom%. It can be seen from Tables 4 and 5 that with an increase in the refractive index (decrease of the N_2O/SiH_4 flow ratio) the nitrogen and the silicon content increased.

From the valences of silicon (+4), oxygen (−2) and nitrogen (−3), a stoichiometric composition of silicon oxynitride can be predicted, under the assumption that the sum of the positive valences must be equal to that of the negative ones and the sum of all atomic concentrations (Si, N and O) in the layer must be equal to 100. This can be represented by the following equations:

$$4X_{Si} = 3X_N + 2X_O \quad (4)$$

$$X_{Si} + X_N + X_O = 100 \quad (5)$$

where X_{Si}, X_O and X_N represent the atomic percentages of silicon, oxygen and nitrogen in the silicon oxynitride layer, respectively.

Table 5
Binding energies of the photoelectron peaks Si 2p, N1s and O1s, the relative atomic concentrations and the empirical formula of the 5 different SiO_xN_y:H layers studied

Sample	Binding energy (eV)			Atomic (%)			Empirical formula
	Si 2p	N1s	O1s	Si	O	N	
S1	103.3	398.4	532.6	32.9	65.0	2.1	$SiO_{1.97}N_{0.06}$
S2	103.0	398.1	332.2	34.0	61.4	4.6	$SiO_{1.80}N_{0.13}$
S3	102.8	398.0	532.2	34.1	59.3	6.6	$SiO_{1.74}N_{0.19}$
S4	102.4	398.0	532.2	35.8	56.0	8.2	$SiO_{1.57}N_{0.23}$
S5	102.3	398.0	532.1	37.9	52.9	9.2	$SiO_{1.40}N_{0.24}$

With the aid of Eqs. (4) and (5) it is possible to derive the silicon and oxygen atomic percentages from the nitrogen atomic percentage according to the following equations:

$$X_{Si} = \frac{100}{3} + \frac{1}{6}X_N \quad (6)$$

$$X_O = \frac{200}{3} - \frac{7}{6}X_N \quad (7)$$

With these equations the silicon or oxygen atomic percentage can now be plotted as a function of the nitrogen atomic percentage for stoichiometric silicon oxynitride as shown in Fig. 1(a) and (b) respectively. For comparison we include also the experimental data points determined by XPS for our 5 layers.

Layers with low nitrogen concentration (lower refractive index, high N_2O/SiH_4 flow ratio) show good agreement between XPS data and the stoichiometric model. Higher refractive index layers with $N_2O/SiH_4 < 20$ deviate increasingly from the stoichiometry. This deviation can be attributed to the formation of silicon rich–silicon oxynitride (step 2). For a quantitative analysis of the Si–Si bonds in the layers, a deconvolution of the Si 2p XPS spectra was performed, see Table 6. Clearly the position of the Si 2p (SiO_xN_y) peak varies from 103.2 eV (sample S1) to 102.3 eV (sample 5). It is well known that the binding energy of Si 2p in the pure silicon is 99.3 eV [24,25]. However this energy is shifted when silicon is bonded with other elements. For Si_3N_4 the Si 2p peak position is at 102 eV (a shift of 2.7 eV from silicon) and for SiO_2 at 103.3 eV (a shift of 4.0 eV) [25]. For SiO_xN_y the Si 2p peak can be expected to have a position between 102 eV and 103.3 eV, the actual position being dependent on the x and y values of the SiO_xN_y compound. The larger the y is, the closer it is to 102 eV, which is in agreement with our calculated empirical formulas of the studied samples (Table 5). The Si 2p peaks of sample S1 and S2 are well fitted with one Gaussian–Lorentzian shaped peak, while other samples (S3, S4 and S5) needed two Gaussian–Lorentzian peaks for fitting (Fig. 2(a) and (b)). The additional

Table 6
Results of the Si 2p peak fitting with relative binding energies (BE), the full width at half maximum (FWHM) and the corrected Si atomic concentration ratio of the 5 different SiO_xN_y:H layers studied

Sample	Si 2p peak					
	Si bonded as SiO_xN_y			Si bonded as ≡Si–Si≡		
	BE (eV)	FWHM (eV)	Atomic (%)	BE (eV)	FWHM (eV)	Atomic (%)
S1	103.2	2.7	32.9	–	–	0.0
S2	102.9	2.8	34.0	–	–	0.0
S3	102.8	2.8	33.9	99.4	1.1	0.2
S4	102.6	2.7	34.6	99.5	1.4	1.2
S5	102.3	2.8	34.7	99.8	2.4	3.2

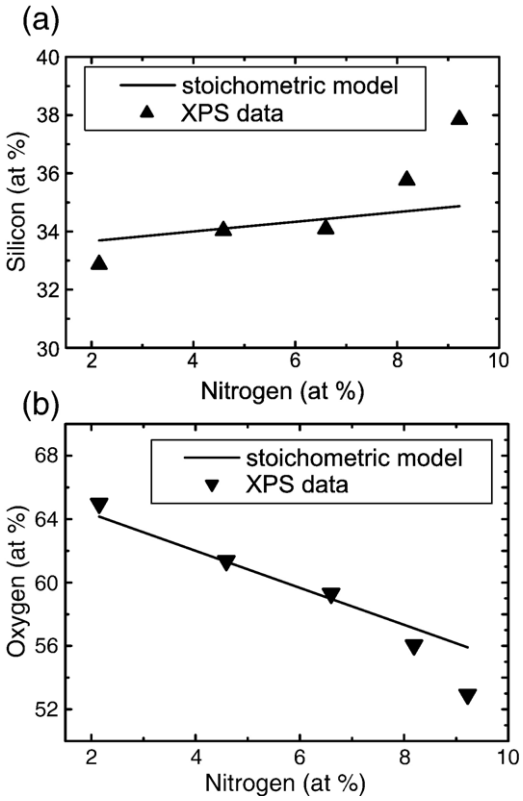

Fig. 1. Atomic percentage of the 5 SiO_xN_y:H layers studied: (a) silicon and (b) oxygen as function of nitrogen concentration. The solid line represents stoichiometric SiO_xN_y, the triangles are experimental data points obtained by XPS.

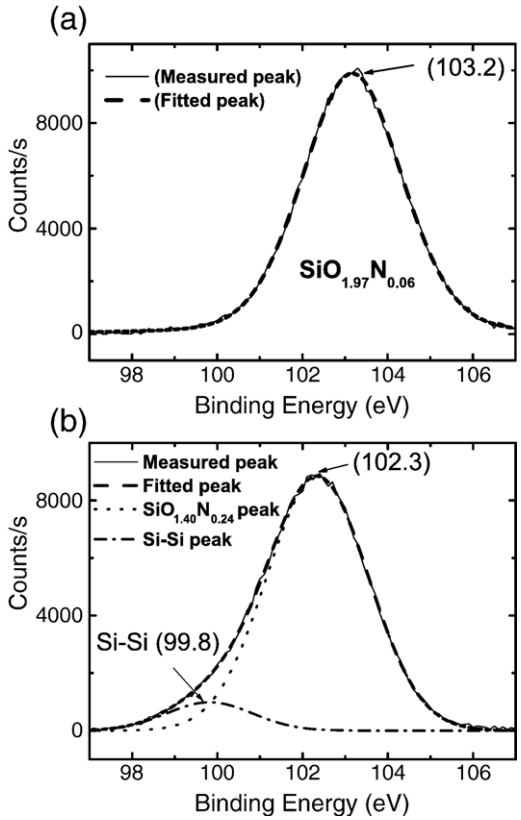

Fig. 2. XPS Si 2p peak fitting for the measured spectrum collected for SiO_xN_y:H (a) sample S1 (b) sample S5.

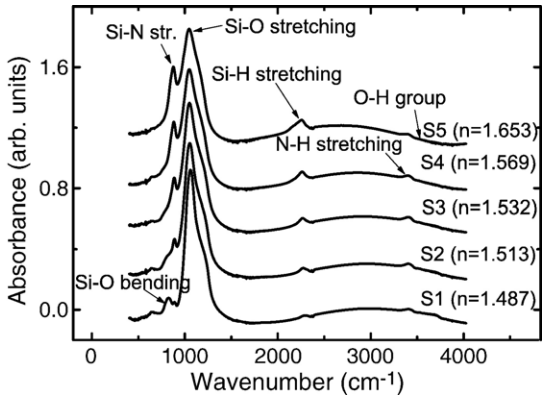

Fig. 3. FTIR spectra of PECVD SiO_xN_y:H layers S1 to S5 with different refractive indices (for better visibility curves are plotted with an offset with respect to each others).

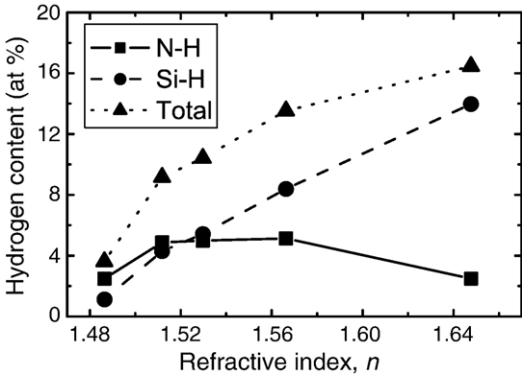

Fig. 5. Hydrogen content as a function of the refractive index for SiO_xN_y:H samples S1–S5.

peaks at 99.4, 99.5 and 99.8 eV were attributed to excess silicon (≡Si−Si≡) in sample S3, S4 and S5 respectively.

FTIR-spectroscopy has been performed on layers with the same composition as given in Table 5 (S1 to S5) to obtain direct information about compositional and vibrational properties of the deposited layers. The FTIR absorption spectra of the layers are shown in Fig. 3. The dominant feature in these spectra is a broad Si–O stretching mode, which occurs at slightly decreasing position (1054, 1046, 1044, 1040 and 1038 cm^{-1}) with an increasing refractive index in the film from samples S1 to S5. The shift in position to higher energy with increasing oxygen content can be attributed to the increase of the electronegativity in the neighborhood of these bonds [6]. The increase in the peak width with the refractive index can be explained by the appearance of Si–N stretching bonds at 870 cm^{-1} at increasing nitrogen content.

The absorption peak at around 820 cm^{-1} in sample S1 is due to the Si–O bending mode. It is due to the excess amount of oxygen in this low index layer that makes the occurrence of Si–O bonds in two different forms (stretching and bending) more probable.

The absorption due to N–H stretching modes in the regions 3300–3400 cm^{-1} and that due to Si–H stretching modes in the regions 2150–2300 cm^{-1} are observed in all samples (S1 to S5). The vibrational overtones of these bonds are well known for their contribution to optical loss at the third telecommunication window around 1550 nm wavelength. It is therefore important to quantify the atomic concentration of hydrogen connected with the N–H and Si–H bonds in the layers.

Like others [26,27] we assume that the presence of N–N, O–O, H–H and N–O bonds in SiON can be excluded due to the high bond strength in N_2, O_2, H_2 and NO molecules, respectively. Also our XPS studies have shown no evidence for N–N and N–O bonds in the layers. Deconvolution of N 1s XPS spectra obtained for sample S1 and S5 have shown the presence of two nitrogen peaks (Fig. 4). The peaks at 397.7 and 397.2 eV have been attributed to $N(-Si)_3$ and those at 398.6 and 398.1 to $Si–N(-H)_2$ for sample S1 and sample S5 respectively [28]. Therefore only Si-centred structures need to be considered. Consequently, taking into account the valences for Si, N, O, and

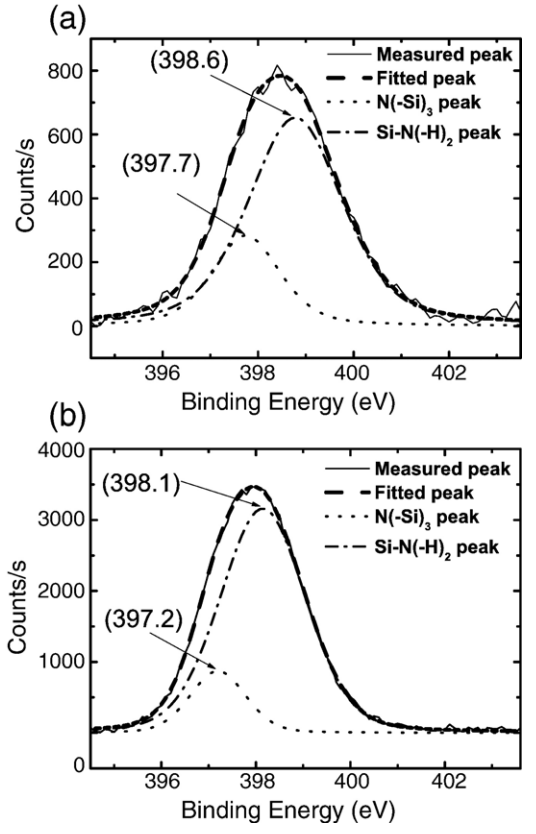

Fig. 4. Deconvolution of N 1s XPS spectra for SiO_xN_y:H (a) sample S1 (b) sample S5.

Table 7
Optical losses and atomic concentration of the 5 different SiO_xN_y:H layers studied

Sample	Gas flow ratio N_2O/SiH_4	Si bonded as Si–Si (at %)	H (at %)	α @ 632.8 nm (dB/cm)	α @ 1550 nm (dB/cm)
S1	75.0	0.0	3.6	<0.2	1.20
S2	39.3	0.0	9.2	<0.2	1.68
S3	28.1	0.2	10.4	0.8	1.82
S4	19.4	1.2	13.5	6.9	2.41
S5	12.5	3.2	16.5	27.7	2.90

H the atomic and bond concentrations are related by the following equations [29]:

$$4[\mathrm{Si}] = 2[\mathrm{Si{-}Si}] + [\mathrm{Si{-}O}] + [\mathrm{Si{-}N}] + [\mathrm{Si{-}H}]$$
$$3[\mathrm{N}] = [\mathrm{Si{-}N}] + [\mathrm{N{-}H}]$$
$$2[\mathrm{O}] = [\mathrm{Si{-}O}] + [\mathrm{O{-}H}]$$
$$1[\mathrm{H}] = [\mathrm{Si{-}H}] + [\mathrm{N{-}H}] + [\mathrm{O{-}H}] \quad (8)$$

O–H vibrations (~3500 cm^{-1}) were not detected by the FTIR; therefore the total hydrogen content according to Eq. (8) can be described in the following way:

$$[\mathrm{H}] = [\mathrm{Si{-}H}] + [\mathrm{N{-}H}] \quad (9)$$

The N–H and Si–H bonds concentrations were determined from the FTIR measurements for all SiO_xN_y:H layers (S1 to S5) by using the method of Lanford and Rand [12] with the aid of the following expression

$$[X{-}H] = \frac{1}{2.303\sigma_{X-H}} \times \int_{band} a(\omega)d\omega \quad (10)$$

where σ_{X-H} is the absorption cross-sections for N–H and Si–H bonds, $a(\omega)d\omega$ is the normalized absorption band area and $a = \left(\frac{2.303}{d}\right)A$ is the absorption coefficient, A being the absorbance and d the film thickness. The absorption cross-sections used in our calculation are $\sigma_{N-H}=5.3\times10^{-18}$ cm^2 and $\sigma_{Si-H}=7.4\times10^{-18}$ cm^2 for N–H and Si–H bonds respectively. The results are plotted in Fig. 5. It appears that the total hydrogen content in the layers increases with increasing n and decreasing gas flow ratio (N_2O/SiH_4). Except for layers S1 and S2, the bonded hydrogen in SiO_xN_y:H is dominant in the form of Si–H bonds, which is in line with the PECVD process mechanisms (step 2).

It can be clearly seen in Fig. 5 that the number of N–H bonds in the layers increases from layer S1 to S2 and decreases at larger n, while the nitrogen concentration is still increasing. We attribute this to the increase of Si–N bonds concentration as the gas flow ratio (N_2O/SiH_4) decreases. In the case of sample S1 and S2 there are sufficient oxygen radicals in the plasma and Si is preferably bonded as Si–O rather than Si–N (step 2), hence most of the nitrogen is bonded as N–H. When the gas flow ratio (N_2O/SiH_4) decreases the oxygen radicals in the reaction decreases too. The formation of Si–N (470 kJ/mol) will become more preferable over N–H (339 kJ/mol) in the gas phase (Table 2). On the other hand, N–H and Si–H bonds may react on the surface to form Si–N (Eq. (3)).

The most important parameter for integrated optics application is the optical loss (α). In addition, loss measurements are very sensitive to the presence of hydrogen and excess silicon. The loss of PECVD SiO_xN_y:H (S1 to S5) slab-type waveguides structure has been determined by using a moving prism in/out-coupling technique. The measurements were performed on the fundamental TE modes at two wavelengths, 632.8 and 1550 nm. The measurement results are given in Table 7. It appears that the optical loss increases for both wavelengths with decreasing gas flow ratio (N_2O/SiH_4). The increase of the optical loss at 632.8 nm can be attributed to the increase in silicon content beyond stoichiometry and therefore increasing concentration of Si–Si bonds. These losses at visible light can be reduced by adding NH_3 to the (N_2O+SiH_4/N_2) gas mixture. In this way the probability of Si–Si bonds formation is reduced since Si is more likely to be bonded to nitrogen than to silicon. Layers with a composition similar to S3, S4 and S5 have been prepared with the addition of NH_3 as process gas and losses below 0.2 dB/cm could be measured indicating the absence of excess silicon.

The optical loss at 1550 nm increases steadily with the hydrogen content. This is the well known effect of the first and the second overtones of the N–H and Si–H frequencies respectively. By a post deposition thermal treatment [2,4,5,8,10] the hydrogen can be removed and the losses at 1550 nm can be reduced to below 0.2 dB/cm. Recent experiments on phosphorus doping of SiON layers show that a significant reduction can be obtained in the hydrogen bonds concentration as well as the optical loss at 1550 nm, when compared to the undoped samples [9].

4. Conclusions

The optical properties of SiON layers were found to depend largely on the deposition parameters, especially on the N_2O/SiH_4 gas flow ratio. The concentrations of the PECVD SiO_xN_y:H layers deposited with high N_2O/SiH_4 flow ratio (>20) can be described with the SiO_xN_y stoichiometric model. The deviation from the stoichiometric composition at lower N_2O/SiH_4 gas flow ratio is due to the formation of silicon rich silicon oxynitride. An increase of silicon content in the layers is accompanied by an increase in the number of Si–H bonds. The excess of silicon and the hydrogen content are responsible for raising the optical losses in the layers at wavelengths of 632.8 and 1550 nm, respectively. Both silicon and hydrogen increase with decreasing N_2O/SiH_4 gas flow ratio.

References

[1] G.L. Bona, R. Germann, B.J. Offrein, IBM J. Res. Develop. 47 (2003) 239.
[2] R. Germann, H.W.M. Salemink, R. Beyeler, G.L. Bona, F. Horst, I. Massarek, B.J. Offrein, J. Electrochem. Soc. 147 (2000) 2237.
[3] C.K. Wong, H. Wong, C.W. Kok, M. Chan, J. Cryst. Growth 288 (2006) 171.
[4] K. Wörhoff, L.T.H. Hilderink, A. Driessen, P.V. Lambeck, J. Electrochem. Soc. 149 (2002) F85.
[5] A.L. Zhang, K.T. Chan, M.S. Demokan, V.W.C. Chan, P.C.H. Chan, A.H.P. Chan, Appl. Phys. Lett. 87 (2005) 101105.
[6] J. Campmany, J.L. Andujar, A. Canillas, J. Costa, E. Bertran, Appl. Surf. Sci. 70/71 (1993) 695.
[7] M. Futatsudera, T. Kimura, A. Matsumoto, T. Inokuma, Y. Kurata, S. Hasegawa, Thin Solid Films 424 (2003) 148.
[8] M.G. Hussein, K. Wörhoff, C.G.H. Roeloffzen, L.T.H. Hilderink, R.M. de Ridder, A. Driessen, in: H. Thienpont, F. Berghmans, J. Danckaert, L. Desmet (Eds.), Proceedings of the Sixth Annual Symposium of the IEEE/LEOS Benelux Chapter, Brussels, Belgium, December 3rd, 2001, p. 265.
[9] M.G. Hussein, K. Worhoff, G. Sengo, A. Driessen, in: P. Megret, M. Wuilpart, S. Bette, N. Staquet (Eds.), Proceedings of the Sixth Annual Symposium of the IEEE/LEOS Benelux Chapter, Mons, Belgium, December 1–2, 2005, p. 104.
[10] K. Wörhoff, A. Driessen, P.V. Lambeck, L.T.H. Hilderink, P.W.C. Linders, T.J.A. Popma, Sens. Actuators, A, Phys. 74 (1999) 9.
[11] A.L. Edwards, An Introduction to Linear Regression and Correlation, Freeman, New York, 1984.

[12] W.A. Lanford, M.J. Rand, J. Appl. Phys. 49 (1978) 2473.
[13] R.G. Hunsperger, Integrated Optics: Theory and Technology, Springer, Berlin, 2002.
[14] D.R. Cote, S.V. Nguyen, A.K. Stamper, D.S. Armbrust, D. Tobben, R.A. Conti, G.Y. Lee, IBM J. Res. Develop. 43 (1999) 5.
[15] S.M. Rossnagel, J.J. Cuomo, W.D. Westwood, Handbook of Plasma Processing Technology: Fundamentals, Etching, Deposition, and Surface Interaction, Noyes Publications, New Jersey, 1990.
[16] J.M. Austin, S.A.L. Smith, J. Phys. D: Appl. Phys. 6 (1973) 2236.
[17] D.R. Lide, Handbook of Chemistry and Physics, CRC Press LLC, New York, 2004.
[18] M.I. Alayo, I. Pereyra, W.L. Scopel, M.C.A. Fantini, Thin Solid Films 402 (2002) 154.
[19] W.A.P. Claassen, Plasma Chem. Plasma Process 7 (1987) 109.
[20] W.A.P. Claassen, W.G.J.N. Valkenburg, M.F.C. Willemsen, W.M.v.d. Wijgert, J. Electrochem. Soc. 132 (1985) 893.
[21] A. Sassella, A. Borghesi, F. Corni, A. Monelli, G. Ottaviani, R. Tonini, B. Pivac, M. Bacchetta, L. Zanotti, J. Vac. Sci. Technol., A, Vac. Surf. Films 15 (1997) 377.
[22] Y.T. Kim, S.M. Cho, Y.G. Seo, H.D. Yoon, Y.M. Im, D.H. Yoon, Cryst. Res. Technol. 37 (2002) 1257.
[23] B. Chapman, Glow Discharge Processes, John Wiley and Sons Inc., New York, 1980.
[24] J.F. Moulder, F.S. William, P.E. Sobol, D.B. Kenneth, Handbook of X-ray Photoelectron Spectroscopy, Perkin-Elmer Corporation, Physical Electronics Division, Eden Prairie, Minnesota, 1992.
[25] R.P. Vasquez, M.H. Hecht, F.J. Grunthaner, M.L. Naiman, Appl. Phys. Lett. 44 (1984) 969.
[26] C.M.M. Denisse, K.Z. Troost, J.B.O. Elferink, F.H.P.M. Habraken, M. Hendriks, J. Appl. Phys. 60 (1986) 2536.
[27] A. Sassella, Phys. Rev., B 48 (1993) 14208.
[28] J.R. Shallenberger, D.A. Cole, S.W. Novak, J. Vac. Sci. Technol., A, Vac. Surf. Films 17 (1999) 1086.
[29] Y. Cros, J.C. Rostaing, J. Peisner, G. Leveque, C. Ance, J. Appl. Phys. 62 (1987) 4538.